NANO LETTERS

Letter

pubs.acs.org/NanoLett

Nanocavity Integrated van der Waals Heterostructure Light-Emitting Tunneling Diode

Chang-Hua Liu,[†] Genevieve Clark,[‡] Taylor Fryett,[§] Sanfeng Wu,[†] Jiajiu Zheng,[§] Fariba Hatami,[∥] Xiaodong Xu,*[,†,‡] and Arka Majumdar*[,†,§]

[†]Department of Physics, [‡]Department of Materials Science and Engineering, and [§]Department of Electrical Engineering, University of Washington, Seattle, Washington 98195, United States

[∥]Department of Physics, Humboldt University, D-12489 Berlin, Germany

Supporting Information

ABSTRACT: Developing a nanoscale, integrable, and electrically pumped single mode light source is an essential step toward on-chip optical information technologies and sensors. Here, we demonstrate nanocavity enhanced electroluminescence in van der Waals heterostructures (vdWhs) at room temperature. The vertically assembled light-emitting device uses graphene/boron nitride as top and bottom tunneling contacts and monolayer WSe_2 as an active light emitter. By integrating a photonic crystal cavity on top of the vdWh, we observe the electroluminescence is locally enhanced (>4 times) by the nanocavity. The emission at the cavity resonance is single mode and highly linearly polarized (84%) along the cavity mode. By applying voltage pulses, we demonstrate direct modulation of this single mode electroluminescence at a speed of ∼1 MHz, which is faster than most of the planar optoelectronics based on transition metal chalcogenides (TMDCs). Our work shows that cavity integrated vdWhs present a promising nanoscale optoelectronic platform.

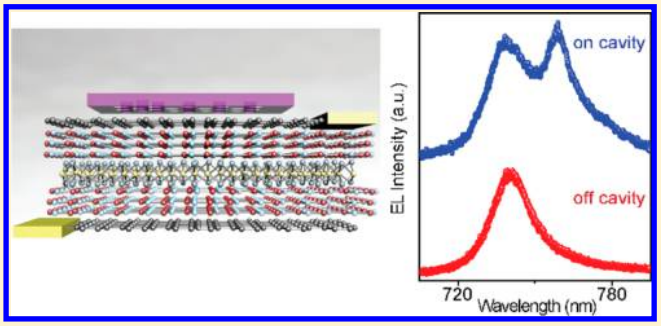

KEYWORDS: *Electroluminescence, van der Waals heterostructure, transition metal dichalcogenides, photonic crystal cavity, optoelectronics*

A nanoscale single-mode light-emitting diode (LED) is a key element for the next generation of integrated nanophotonics.[1] Over the past two decades, there have been tremendous efforts toward realizing compact, efficient, scalable, and electrically driven light emitters, which can be integrated with other active or passive elements on a chip and can function at room temperature.[1,2] Thus far, diverse optoelectronic materials, ranging from bulk III−V and Ge to low-dimensional nanomaterials, such as quantum wells, dots, or nanowires, have been extensively explored and applied as the photonic sources with different functionalities.[3−6] However, the efficiency, cost of integration, and modulation speed is still far from the desired performance, and new materials need to be explored. Atomically thin monolayer transition metal dichalcogenides (TMDCs) are a new class of materials with strong light-matter interaction and can be easily transferred to any substrate without needing explicit lattice matching,[7] emerging as a promising material system for integrated photonic applications.[7−9]

The initial investigations of electronic properties and excitonic effects of 2D TMDCs have opened up the development of atomically thin electrically driven light emitters, based on the simple transistors or lateral p−n junctions.[10−16] Continued efforts further demonstrated that different 2D materials can be vertically assembled into vdWhs,[17] leading to more efficient and larger area of light emission.[13,18−20] On the other hand, the emission from the TMDCs can be further enhanced by using a nanocavity, due to spatial and spectral confinement of light. Initial experiments with cavity integrated TMDCs have shown operation of strongly coupled exciton−polaritons at room temperature[21,22] and optically pumped nanolasers.[23−25] Despite the aforementioned progress, it remains challenging to electrically control a 2D light emitter integrated with photonic cavities. Because a single mode light-emitting device is sufficient for many on-chip photonic applications,[6,26] developing a monolayer LED integrated with nanocavity will be important and desirable for practical applications. In this paper, we demonstrate such a device based on the integration of a light emitter formed by vdWh tunneling diode with a photonic crystal nanocavity. We observe cavity-enhanced electroluminescence with high degree of linear polarization along the cavity mode at room temperature. We further demonstrate the electrical modulation of the resulting single mode light-emitting device at a speed of ∼1 MHz.

Figures 1a−c shows the optical image and schematic of the light-emitting device. The heterostructure is composed of a

Received: September 9, 2016
Revised: December 6, 2016
Published: December 7, 2016

DOI: 10.1021/acs.nanolett.6b03801
Nano Lett. XXXX, XXX, XXX−XXX

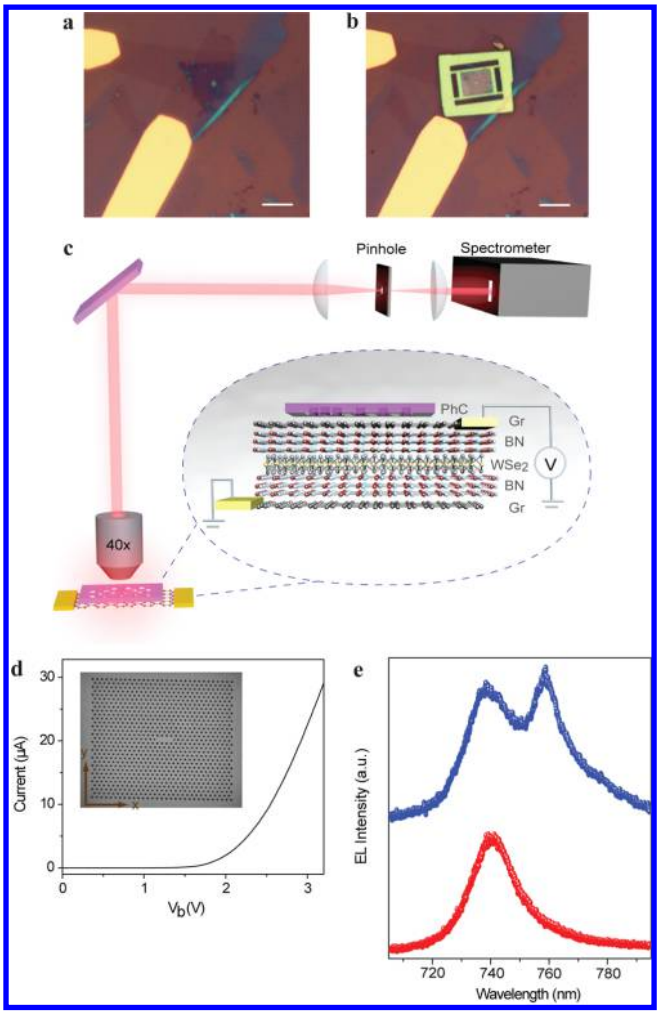

Figure 1. Device and signature of cavity coupled EL. (a) Optical microscope images of the light-emitting van der Waals heterostructures and (b) its integration with a photonic crystal cavity. Scale bar: 5 μm. (c) Schematic of the EL measurement setup and device architecture. (d) $I-V$ characteristics of the light-emitting heterostructure. Inset: Scanning electron microscopy image of the photonic crystal cavity. (e) EL measured from (blue dots) and away (red dots) from the cavity area with V_b = 2 V.

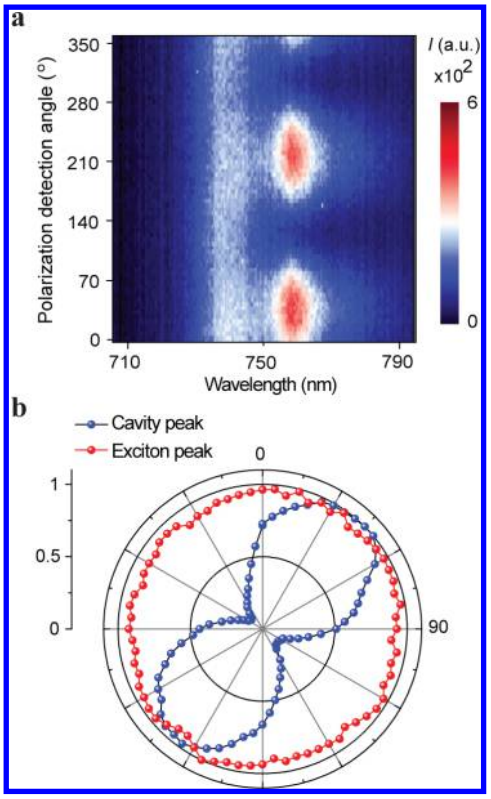

Figure 2. Polarization resolved electroluminescence. (a) Measured on-cavity EL as a function of polarization detection angle. The bias voltage is 1.8 V. (b) Normalized cavity-enhanced peak intensity (blue dots) and exciton peak intensity (red dots) as a function of polarization detection angle.

monolayer tungsten diselenide (WSe_2) sandwiched by two tunneling contacts formed by graphene/mono or bilayer hexagonal boron nitride (hBN). The WSe_2 is chosen as the active light-emitting layer since its emission efficiency is stronger at room temperature compared to the low temperature because WSe_2 has dark exciton states below bright exciton.[20,27] After assembling this 2D heterostructure, a photonic crystal slab made of gallium phosphide (Figure 1d, inset) was precisely aligned and transferred onto the light-emitting WSe_2 area as shown in Figure 1b (see Supporting Information for device fabrication).

By applying the bias voltage across two graphene layers, electrons and holes tunnel from the top and bottom graphene layers into WSe_2, leading to $I-V$ characteristics in Figure 1d. The injected electrons and holes stay in the WSe_2 for a finite time and form excitons, which then radiatively recombine and give rise to electroluminescence (EL). To identify the effect of photonic crystal cavity on EL, a confocal pinhole was setup in the light collection path (Figure 1c) to spatially resolve the EL spectrum from and off-cavity (Figure 1e). The EL collected from the off-cavity area (red dots) shows a single peak. The EL collected from cavity (blue dots), however, shows an additional narrow peak centered ~759 nm, suggesting the in-plane electric dipoles in WSe_2 can be coupled into the TE mode of the photonic cavity, and more importantly the cavity can enhance the spontaneous emission rate of WSe_2 via Purcell effect.[28,29]

To further confirm that the peak at ~759 nm originated from cavity-enhanced EL, we added a linear polarizer in the light collection path to examine the EL polarization at different detection angles (θ). We have identified that the y-polarized emission from the bare photonic crystal cavity mode is along θ = 40°. As exhibited in Figure 2a, the EL collected spatially from the cavity area, but spectrally detuned from the 759 nm cavity mode, is polarization insensitive. This is distinct from the highly polarized EL at the cavity resonance. More quantitatively, we plot the normalized EL intensity (I), extracted from the exciton peak (738.7 nm) and cavity peak (759 nm), as a function of θ (Figure 2b). The results show that the only EL at 759 nm is linearly polarized along the cavity mode with a degree of polarization ρ = 84%, quantified by the formula $\rho = \frac{I_{max} - I_{min}}{I_{max} + I_{min}}$. These polarization resolved measurements evidently confirm the cavity mode is coupled to the 2D-exciton EL, can control the polarization of light emission, and implies a single mode operation of the LED.

After confirming the cavity coupling with the 2D exciton, we measure the cavity-enhanced EL and the spectral line shape as a function of the bias voltage. Figure 3a presents the EL at four selected bias, detected along and orthogonal to the cavity mode polarization, under different bias voltages (see Supporting

DOI: 10.1021/acs.nanolett.6b03801
Nano Lett. XXXX, XXX, XXX−XXX

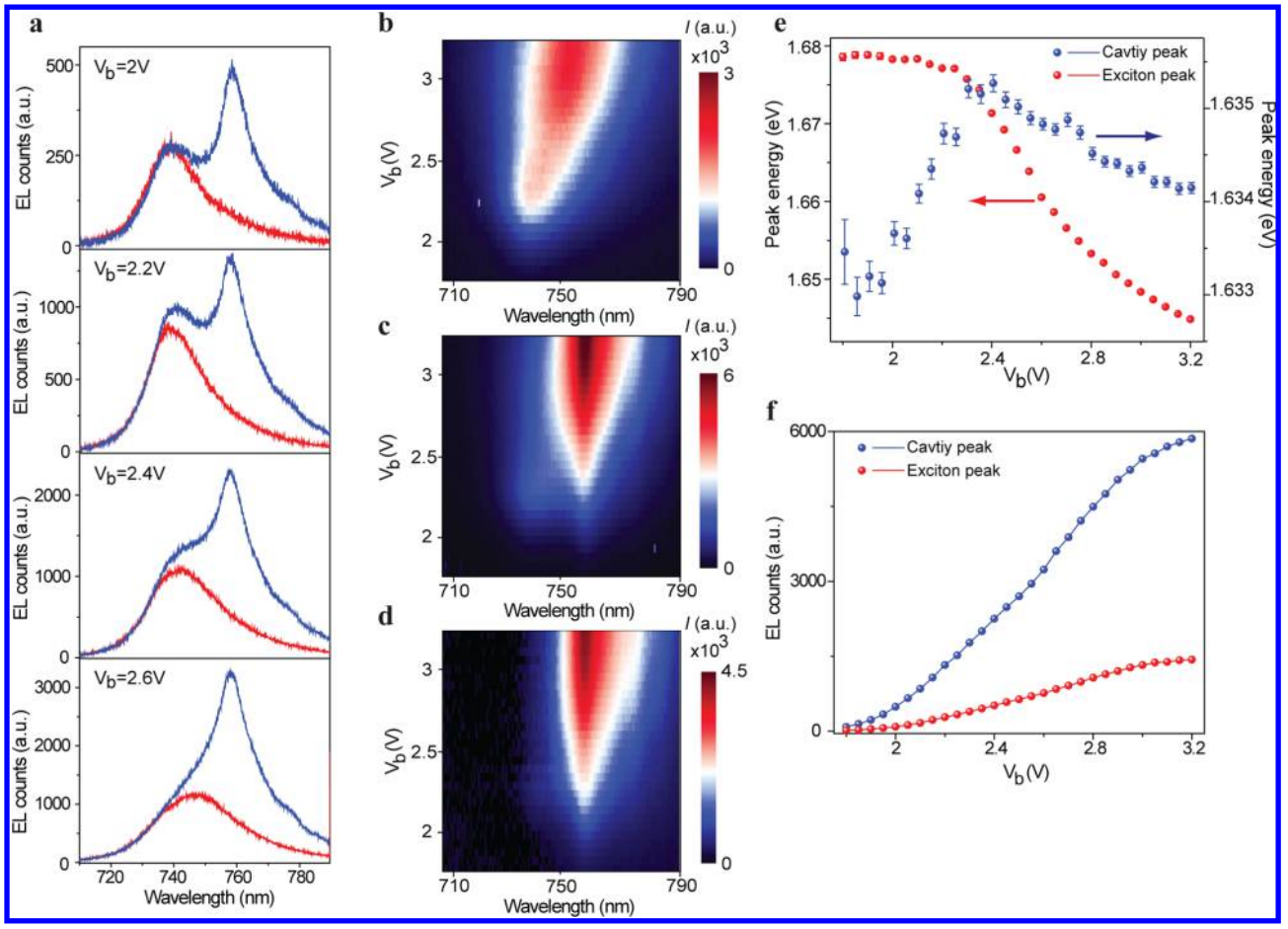

Figure 3. Bias dependent electroluminescence. (a) The cross-polarized EL spectra from the photonic crystal cavity at selected bias voltages. From top to bottom: 2, 2.2, 2.4, and 2.6 V. The blue and red spectra are measured along (*y*-polarized) and orthogonal (*x*-polarized) to the cavity mode, respectively. (b–d) The EL intensity plot as a function of applied bias and emission energy. EL measured (b) orthogonal and (c) along the cavity mode polarization, whose difference shows (d) cavity-enhanced EL. (e) Peak energy of the exciton (red dots) and cavity-enhanced (blue dots) EL versus the bias voltage. (f) Intensity of the exciton (red dots) and cavity-enhanced (blue dots) peaks versus the bias voltage.

Information for all bias-dependent spectra). The evolution of these cross-polarized spectra are also compared in the bias-dependent EL intensity plots (Figure 3b,c). Evidently, these plots again reveal that the cavity selectively enhances the spontaneous emission polarized along the cavity mode polarization, whereas the orthogonally polarized EL is the WSe_2 exciton emission decoupled from the cavity mode. Hence, the cavity-enhanced EL can be obtained by subtracting the co- and cross-polarized EL spectra from each other, as shown in Figure 3d. The full width at half-maximum (fwhm) of cavity peak is of about 10 nm at V_b = 1.8 V and increases as bias (see Supporting Information). This line width is broader than the pristine cavity and is consistent with the finite difference time domain (FDTD) simulations, which suggests that the cavity *Q*-factor degrades when the previously floating photonic crystal is transferred onto the SiO_2.

To gain further insight, we extract the peak energy position of the cavity-decoupled (Figure 3b) and cavity-coupled (Figure 3c) EL spectra and plot them in Figure 3e. Notably, as the bias voltage increases, the peak position of cavity-decoupled EL is red-shifted by about ~33 meV, corresponding to the trion binding energy for WSe_2. This implies the EL changes from neutral to charged exciton emission as bias increases.[30] For the cavity-coupled peak, the shift is relatively small (less than 2 meV), because it is fixed by the cavity mode, and exhibits a distinct turnover from the blue to red shift near V_b = 2.4 V (Figure 3e, blue dots). These signatures suggest the photonic crystal cavity is subjected to the free carrier and joule heating effects, leading to slightly blue and red shifts, as widely reported in literature.[31,32] In addition to the peak energy, the amplitudes of cavity-decoupled and cavity-coupled peaks versus bias voltages are also extracted from Figure 3b,c, respectively. As plotted in Figure 3f, when applying the higher bias voltage, the cavity-coupled peak increases rapidly. This is likely due to that the weight of EL shifts to trion states as bias increases, whose energy is nearly resonant with the cavity mode. The EL peak amplitude can be enhanced by more than 4 times compared with the cavity-decoupled peak. Given the cavity quality factor (~100) and the mode volume of this device $\left(\sim 0.7\left(\frac{\lambda}{n}\right)^3 \right)$, we expect that the enhancement can reach 10, which is larger than what we measure. However, we note that the real peak enhancement ratio can be higher because the confocal pinhole detection might collect part of the EL from the vicinity of photonic crystal cavity.

In addition to the polarization analysis, we perform the spatially resolved EL to verify the cavity enhancement effect. Figure 4a presents a 2D map of integrated EL with the device biased at 2.7 V. The map shows the stronger emission in the center of cavity region. To further separate cavity-enhanced EL,

DOI: 10.1021/acs.nanolett.6b03801
Nano Lett. XXXX, XXX, XXX−XXX

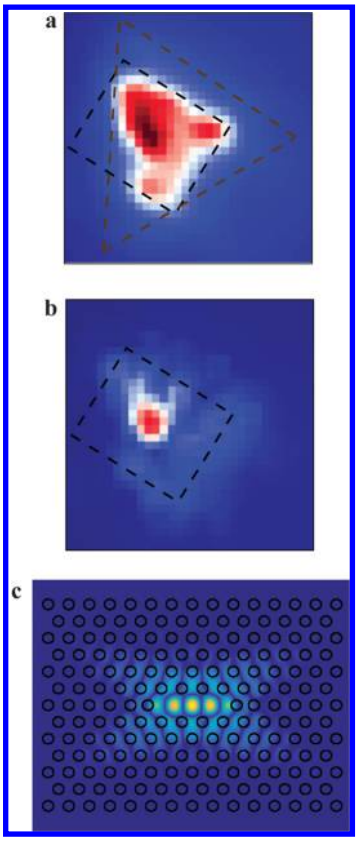

Figure 4. Spatially resolved cavity-enhanced electroluminescence. The 2D map of the integrated EL (a) without and (b) with polarization distinction showing only cavity-enhanced EL within a spectral window from 710 to 785 nm at a bias voltage of 2.7 V. The black and brown dashed lines indicate the area of photonic crystal and WSe_2 respectively. (c) Simulated electric field mode profile of the L3 type photonic crystal cavity.

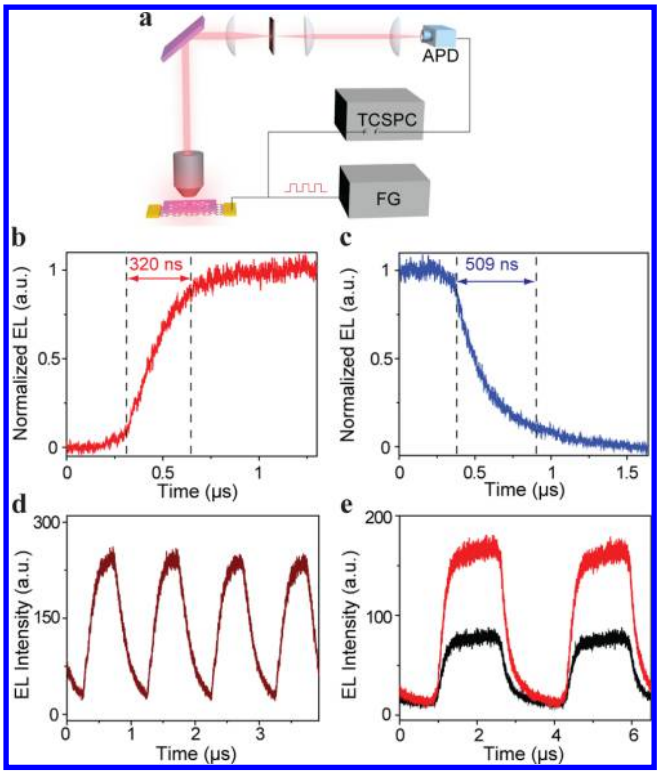

Figure 5. Direct electrical modulation of electroluminescence. (a) Schematic of EL modulation and time-resolved measurement. APD: avalanche photodiode. TCSPC: Time-correlated single photon counter. FG: Function generator. (b,c) Characterization the device response time. (b) Rise time and (c) decay time, when electrically turning on and off the light emitter, respectively. (d) Demonstration of 1 MHz electrical switch of the light emitter. (e) EL modulation at 300 kHz with the amplitude of voltage pulses at 2.4 (black) and 2.8 V (red) respectively.

we again measure the cross-polarized (θ = 40° and θ = 130°) EL spectra over the entire device. The difference of integrated EL map with orthogonal polarization was then calculated and plotted in Figure 4b. Evidently, the map shows that the cavity mode profile is spatially localized, and therefore the spontaneous emission is enhanced within heterostructure below the photonic crystal cavity. The results agree with the electric field distribution simulated by FDTD shown in Figure 4c and, more importantly, highlight that our device configuration can be a feasible platform to hybridize an electrically pumped emitter, based on TMDCs, with the photonic crystal nanocavities.

Finally, we probe direct electrical modulation of the light-emitting device. Figure 5a depicts the measurement setup. Voltage pulses generated from a function generator modulate the EL from the device, which is detected by an avalanche photodiode (APD). The electrical signals generated from APD and function generator were then sent to a time-correlated single photon counter, which measured the delay between photon arrival times to the APD and the applied voltage pulses. On the basis of this time-resolved measurement, the transient rise as well as decay of EL upon turning on and off the voltage pulses were resolved in Figure 5b,c. By extracting the time intervals between 10−90% (90−10%) of the maximum EL intensity, the rise and fall times are estimated to be ∼320 and ∼509 ns, implying the operational cutoff speed of the device ∼1 MHz (Figure 5d). Moreover, by varying the amplitude of input voltage pulses, the EL on/off ratio of the device can be increased while keeping the same rise/fall time and EL intensity during the off-pulse section (Figure 5e). Such direct modulation of the EL is a prerequisite for many integrated photonic applications related to optical interconnects.[33] Additionally, such modulated light source will find applications in miniature optical sensors or display, where ultrahigh speed is not an absolute necessity. We emphasize that the operation speed of our device is much faster than most of the planar LEDs or photodetectors based on TMDCs,[8,34] because the injection of carriers relies on ultrafast tunneling (∼ps)[35] without suffering from low mobility in TMDCs or Schottky junctions near the metal contacts. We note the current 1 MHz is limited by the RC time constant (see Supporting Information) and therefore reducing the parasitic capacitance and improving device architecture have the potential to further enhance the operation speed to approximately gigahertz at room temperature, ultimately limited by the radiative recombination time (∼ns).[27]

In summary, we demonstrated a viable route for integrating a photonic crystal cavity with an electrically driven light emitter based on vdWhs. The resulting light-emitting devices can be readily operated at room temperature with fast modulation speed. With this framework, the photonic sources with different operational wavelengths can also be achieved by replacing WSe_2 with other 2D optoelectronic materials.[7] Furthermore, we estimate our present light emitter has quantum efficiency below 0.2% (see Supporting Information). We anticipate improving the quantum efficiency of light emitter, for example, chemical

DOI: 10.1021/acs.nanolett.6b03801
Nano Lett. XXXX, XXX, XXX−XXX

treatments,[36,37] and using high-Q cavity will further increase the cavity enhancement and possibly lead to electrically pumped lasing behavior.

■ ASSOCIATED CONTENT

Supporting Information

The Supporting Information is available free of charge on the ACS Publications website at DOI: 10.1021/acs.nanolett.6b03801.

Detailed device fabrication, characterization and simulation of photonic crystal cavity, photoluminescence measurements, bias-dependent electroluminescence, and estimation of device speed limit and external quantum efficiency (PDF)

■ AUTHOR INFORMATION

Corresponding Authors

*E-mail: xuxd@uw.edu.
*E-mail: arka@uw.edu.

ORCID

Chang-Hua Liu: 0000-0001-8042-9218
Sanfeng Wu: 0000-0002-6227-6286
Jiajiu Zheng: 0000-0003-1527-201X

Author Contributions

X.X. and A.M. conceived and supervised the projects. T.F. and J.Z. fabricated, simulated, and characterized the photonic crystal cavities. G.C. grew monolayer WSe_2 and fabricated and characterized the van der Waals light-emitting device. C.L. fabricated the cavity-integrated device and carried out the experiments, assisted by G.C. and S.W. F.H. grew the GaP membrane. C.L., X.X., and A.M. analyzed the results and wrote the paper. All authors discussed the results.

Notes

The authors declare no competing financial interest.

■ ACKNOWLEDGMENTS

This work is supported by the National Science Foundation under Grant NSF-EFRI-1433496, the Air Force Office of Scientific Research-Young Investigator Program under Grant FA9550-15-1-0150, and AFOSR (FA9550-14-1-0277). The cavity fabrication was performed at the Washington Nanofabrication Facility (WNF), a National Nanotechnology Infrastructure Network (NNIN) site at the University of Washington, which is supported in part by the National Science Foundation (awards 0335765 and 1337840), the Washington Research Foundation, the M. J. Murdock Charitable Trust, GCE Market, Class One Technologies, and Google. X.X. acknowledges the support by Boeing Distinguished Professorship and from the State of Washington funded Clean Energy Institute.

■ REFERENCES

(1) Miller, D. A. B. *Proc. IEEE* **2009**, *97*, 1166−1185.
(2) Liang, D.; Bowers, J. E. *Nat. Photonics* **2010**, *4*, 511−517.
(3) Shields, A. J. *Nat. Photonics* **2007**, *1*, 215−223.
(4) Yan, R.; Gargas, D.; Yang, P. *Nat. Photonics* **2009**, *3*, 569−576.
(5) Ellis, B.; Mayer, M. A.; Shambat, G.; Sarmiento, T.; Harris, J.; Haller, E. E.; Vuckovic, J. *Nat. Photonics* **2011**, *5*, 297−300.
(6) Shambat, G.; Ellis, B.; Majumdar, A.; Petykiewicz, J.; Mayer, M. A.; Sarmiento, T.; Harris, J.; Haller, E. E.; Vuckovic, J. *Nat. Commun.* **2011**, *2*, 539.
(7) Xia, F.; Wang, H.; Xiao, D.; Dubey, M.; Ramasubramaniam, A. *Nat. Photonics* **2014**, *8*, 899−907.
(8) Mak, K. F.; Shan, J. *Nat. Photonics* **2016**, *10*, 216−226.
(9) Wang, Q. H.; Kalantar-Zadeh, K.; Kis, A.; Coleman, J. N.; Strano, M. S. *Nat. Nanotechnol.* **2012**, *7*, 699−712.
(10) Sundaram, R. S.; Engel, M.; Lombardo, A.; Krupke, R.; Ferrari, A. C.; Avouris, P.; Steiner, M. *Nano Lett.* **2013**, *13*, 1416−1421.
(11) Jo, S.; Ubrig, N.; Berger, H.; Kuzmenko, A. B.; Morpurgo, A. F. *Nano Lett.* **2014**, *14*, 2019−2025.
(12) Zhang, Y. J.; Oka, T.; Suzuki, R.; Ye, J. T.; Iwasa, Y. *Science* **2014**, *344*, 725−728.
(13) Withers, F.; Del Pozo-Zamudio, O.; Mishchenko, A.; Rooney, A. P.; Gholinia, A.; Watanabe, K.; Taniguchi, T.; Haigh, S. J.; Geim, A. K.; Tartakovskii, A. I.; Novoselov, K. S. *Nat. Mater.* **2015**, *14*, 301−306.
(14) Baugher, B. W. H.; Churchill, H. O. H.; Yang, Y.; Jarillo-Herrero, P. *Nat. Nanotechnol.* **2014**, *9*, 262−267.
(15) Pospischil, A.; Furchi, M. M.; Mueller, T. *Nat. Nanotechnol.* **2014**, *9*, 257−261.
(16) Ross, J. S.; Klement, P.; Jones, A. M.; Ghimire, N. J.; Yan, J.; Mandrus, D. G.; Taniguchi, T.; Watanabe, K.; Kitamura, K.; Yao, W.; Cobden, D. H.; Xu, X. *Nat. Nanotechnol.* **2014**, *9*, 268−272.
(17) Geim, A. K.; Grigorieva, I. V. *Nature* **2013**, *499*, 419−425.
(18) Clark, G.; Schaibley, J. R.; Ross, J.; Taniguchi, T.; Watanabe, K.; Hendrickson, J. R.; Mou, S.; Yao, W.; Xu, X. *Nano Lett.* **2016**, *16*, 3944−3948.
(19) Cheng, R.; Li, D.; Zhou, H.; Wang, C.; Yin, A.; Jiang, S.; Liu, Y.; Chen, Y.; Huang, Y.; Duan, X. *Nano Lett.* **2014**, *14*, 5590−5597.
(20) Withers, F.; Del Pozo-Zamudio, O.; Schwarz, S.; Dufferwiel, S.; Walker, P. M.; Godde, T.; Rooney, A. P.; Gholinia, A.; Woods, C. R.; Blake, P.; Haigh, S. J.; Watanabe, K.; Taniguchi, T.; Aleiner, I. L.; Geim, A. K.; Fal'ko, V. I.; Tartakovskii, A. I.; Novoselov, K. S. *Nano Lett.* **2015**, *15*, 8223−8228.
(21) Liu, X.; Galfsky, T.; Sun, Z.; Xia, F.; Lin, E.-c.; Lee, Y.-H.; Kena-Cohen, S.; Menon, V. M. *Nat. Photonics* **2014**, *9*, 30−34.
(22) Dufferwiel, S.; Schwarz, S.; Withers, F.; Trichet, A. A. P.; Li, F.; Sich, M.; Del Pozo-Zamudio, O.; Clark, C.; Nalitov, A.; Solnyshkov, D. D.; Malpuech, G.; Novoselov, K. S.; Smith, J. M.; Skolnick, M. S.; Krizhanovskii, D. N.; Tartakovskii, A. I. *Nat. Commun.* **2015**, *6*, 8579.
(23) Wu, S.; Buckley, S.; Schaibley, J. R.; Feng, L.; Yan, J.; Mandrus, D. G.; Hatami, F.; Yao, W.; Vuckovic, J.; Majumdar, A.; Xu, X. *Nature* **2015**, *520*, 69−72.
(24) Ye, Y.; Wong, Z. J.; Lu, X.; Ni, X.; Zhu, H.; Chen, X.; Wang, Y.; Zhang, X. *Nat. Photonics* **2015**, *9*, 733−737.
(25) Salehzadeh, O.; Djavid, M.; Tran, N. H.; Shih, I.; Mi, Z. *Nano Lett.* **2015**, *15*, 5302−5306.
(26) Tsakmakidis, K. L.; Boyd, R. W.; Yablonovitch, E.; Zhang, X. *Opt. Express* **2016**, *24*, 17916−17927.
(27) Zhang, X.-X.; You, Y.; Zhao, S. Y. F.; Heinz, T. F. *Phys. Rev. Lett.* **2015**, *115*, 257403.
(28) Wu, S.; Buckley, S.; Jones, A. M.; Ross, J. S.; Ghimire, N. J.; Yan, J.; Mandrus, D. G.; Yao, W.; Hatami, F.; Vuckovic, J.; Majumdar, A.; Xu, X. *2D Mater.* **2014**, *1*, 011001.
(29) Gan, X.; Gao, Y.; Mak, K. F.; Yao, X.; Shiue, R.-J.; van der Zande, A.; Trusheim, M. E.; Hatami, F.; Heinz, T. F.; Hone, J.; Englund, D. *Appl. Phys. Lett.* **2013**, *103*, 181119.
(30) Jones, A. M.; Yu, H.; Ghimire, N. J.; Wu, S.; Aivazian, G.; Ross, J. S.; Zhao, B.; Yan, J.; Mandrus, D. G.; Xiao, D.; Yao, W.; Xu, X. *Nat. Nanotechnol.* **2013**, *8*, 634−638.
(31) Shambat, G.; Ellis, B.; Mayer, M. A.; Majumdar, A.; Haller, E. E.; Vuckovic, J. *Opt. Express* **2011**, *19*, 7530−7536.
(32) Faraon, A.; Vuckovic, J. *Appl. Phys. Lett.* **2009**, *95*, 043102.
(33) Lau, E. K.; Lakhani, A.; Tucker, R. S.; Wu, M. C. *Opt. Express* **2009**, *17*, 7790−7799.
(34) Lopez-Sanchez, O.; Lembke, D.; Kayci, M.; Radenovic, A.; Kis, A. *Nat. Nanotechnol.* **2013**, *8*, 497−501.
(35) Ma, Q.; Andersen, T. I.; Nair, N. L.; Gabor, N. M.; Massicotte, M.; Lui, C. H.; Young, A. F.; Fang, W. J.; Watanabe, K.; Taniguchi, T.; Kong, J.; Gedik, N.; Koppens, F. H. L.; Jarillo-Herrero, P. *Nat. Phys.* **2016**, *12*, 455−459.
(36) Amani, M.; Lien, D.-H.; Kiriya, D.; Xiao, J.; Azcatl, A.; Noh, J.; Madhvapathy, S. R.; Addou, R.; Santosh, K. C.; Dubey, M.; Cho, K.;

DOI: 10.1021/acs.nanolett.6b03801
Nano Lett. XXXX, XXX, XXX−XXX

Wallace, R. M.; Lee, S.-C.; He, J.-H.; Ager, J. W., III; Zhang, X.; Yablonovitch, E.; Javey, A. *Science* **2015**, *350*, 1065−1068.
(37) Amani, M.; Taheri, P.; Addou, R.; Ahn, G. H.; Kiriya, D.; Lien, D.-H.; Ager, J. W., III; Wallace, R. M.; Jayey, A. *Nano Lett.* **2016**, *16*, 2786−2791.

DOI: 10.1021/acs.nanolett.6b03801
Nano Lett. XXXX, XXX, XXX−XXX